Journal of Sound and Vibration 326 (2009) 263–276

Contents lists available at ScienceDirect

Journal of Sound and Vibration

journal homepage: www.elsevier.com/locate/jsvi

Cantilevered flexible plates in axial flow: Energy transfer and the concept of flutter-mill

Liaosha Tang [a,c,*], Michael P. Païdoussis [b], Jin Jiang [c]

[a] University of Toronto Institute for Aerospace Studies, 4925 Dufferin St., Ontario, Canada M3H 5T6
[b] Department of Mechanical Engineering, McGill University, 817 Sherbrooke St. W., Montréal, Québec, Canada H3A 2K6
[c] Hubei Key Laboratory of Fluid Machinery and Power Equipment Technology, Wuhan University, 8 Donghu St. S., Wuahn, Hubei 430072, PR China

ARTICLE INFO

Article history:
Received 5 May 2008
Received in revised form
15 April 2009
Accepted 29 April 2009
Handling Editor: C.L. Morfey
Available online 4 June 2009

ABSTRACT

Cantilevered flexible plates in axial flow lose stability at sufficiently high flow velocity. Once the instability threshold is exceeded, flutter takes place, and energy is continuously pumped into the plate from the surrounding fluid flow, sustaining the flutter motion. This kind of self-induced, self-sustained vibration can be utilized to extract energy from the fluid flow. This paper studies the energy transfer between the fluid flow and the plate. Then, based on the energy analysis of the fluid–structure interaction system, a new concept of energy-harvesting, the flutter-mill, is proposed in which these flutter motions are utilized to generate electrical power.

1. Introduction

Flutter is not always an unfavourable phenomenon; it can be utilized to do useful work, for example, for the generation of electricity. The oil crisis in the mid-1970s encouraged the pursuit of alternative sources of energy; many designs of *unconventional* energy-harvesting devices utilizing the flutter motions of airfoils/wings came into being at that time. The idea of an oscillating-wing windmill (the so-called wingmill) was proposed by Adamko and DeLaurier [1] and Mckinney and DeLaurier [2]; a prototype of this wind energy converter was developed and tested. When this kind of device is properly designed so as to achieve a $-\pi/2$ phase difference between the plunging and pitching motions, Ly and Chasteau [3] have demonstrated that its efficiency is equivalent to that of the vertical axis (Darrieus-type) wind turbine [4]. The studies on the wingmill continued [5–8], and a patent [9] was recently granted. Unlike the wingmill, which aims to compete with conventional wind turbines, the design of an energy-harvesting eel was proposed by Allen and Smits [10] and Taylor et al. [11] as an electricity source to power small, remotely located, wireless sensors. In the design of energy-harvesting eels, a film made of piezoelectric polymer (i.e., the eel) is put in the wake generated from an upstream bluff body; this device converts the mechanical energy of the wake-induced vibrations to electrical power. A patent has been filed by Carroll [12] for the concept of the energy-harvesting eel; and the project is still under way with the goal of building a prototype capable of generating 1 W electrical power in a 1 m/s water current. Another interesting design for an energy-harvesting device utilizing flow-induced vibrations is the so-called windbelt, which has recently been patented and manufactured by Humdinger Wind Energy, LLC [13]. A windbelt is no more than a properly tensioned flexible belt (say, Mylar-coated taffeta tape) in airflow; different from the above-mentioned wingmill and energy-harvesting eel designs, a

* Corresponding author at: University of Toronto Institute for Aerospace Studies, 4925 Dufferin St., Ontario, Canada M3H 5T6. Tel.: +1 416 6677701; fax: +1 416 6677799.
E-mail address: ltang2008@gmail.com (L. Tang).

0022-460X/$ - see front matter © 2009 Elsevier Ltd. All rights reserved.
doi:10.1016/j.jsv.2009.04.041

key characteristic of the windbelt is the three-dimensional deformations of the flexible belt. It should be mentioned that a similar energy-harvesting device involving three-dimensional deformation of the structure can also be found in the design of the hydro-generator with an elastic oscillating wing proposed by Vortex Oscillating Technology, Ltd. [14].

The dynamics of two-dimensional cantilevered thin flexible plates in subsonic axial flow has recently been reviewed by Tang and Païdoussis [15] in a systematic manner. The two-dimensional plate is modelled as a beam with an inextensible centreline, and an unsteady lumped vortex model is used to calculate the pressure difference across the laterally oscillating plate. The analysis of the system dynamics is carried out in the time-domain. The system is found to lose stability by flutter at sufficiently high flow velocity, and both the instability threshold, as a function of system parameters, and the post-critical behaviour of the system have been extensively studied. The present paper investigates the energy transfer between the plate and the surrounding fluid flow; we not only calculate the total energy transferred from the fluid flow to the plate as an indication of the onset of flutter, but we also break down the total energy transfer in terms of (i) various segments along the length of the plate and (ii) various vibration modes of the plate. Based on energy analysis, the concept of a new energy-harvesting device, the "flutter-mill", is proposed. In the light of the dynamics of the system and the associated pattern of energy transfer, key system parameters of the flutter-mill can be determined. Moreover, the performance of the flutter-mill is preliminarily evaluated and compared to a real horizontal axis wind turbine (HAWT) [16].

2. The fluid-elastic model

A schematic diagram of a cantilevered flexible plate in axial flow is shown in Fig. 1. The geometrical characteristics of the rectangular homogeneous plate are the length of the flexible section L, width B and thickness h; $B \to \infty$ and $h \ll L$ for a two-dimensional thin plate. Normally, there is a rigid segment of length L_0 as part of the clamping arrangement at the upstream end. The other physical parameters of the system are: the plate material density ρ_P and bending stiffness $D = Eh^3/\sqrt{12(1-\nu^2)}$, where E and ν are, respectively, Young's modulus and the Poisson ratio of the plate material, the fluid density ρ_F, and the undisturbed flow velocity U. As shown in Fig. 1, W and V are, respectively, the transverse and longitudinal displacements of the plate; F_L and F_D are the aero/hydrodynamic loads acting on the plate in the transverse and longitudinal directions, respectively; S is the distance of a material point on the plate from the origin, measured along the plate centreline in a coordinate system embedded in the plate. Moreover, material damping of the Kelvin–Voigt-type is considered for the plate, with a loss factor denoted by a.

The equations of motion of the plate can be written in nondimensional form as [15]

$$\frac{1}{\mu U_R^2}\left\{\ddot{w} + \left(1 + \alpha\frac{\partial}{\partial\tau}\right)[w''''(1+w'^2) + 4w'w''w''' + w''^3] - (T^\star w')'\right\} = f_L, \tag{1}$$

$$\nu = -\frac{1}{2}\int_0^s w'^2\,\mathrm{d}s, \tag{2}$$

where the overdot and the prime represent $\partial(\,)/\partial\tau$ and $\partial(\,)/\partial s$, respectively. The nondimensional tension $T^\star$ in the plate is given by

$$T^\star = \int_s^1 (\mu U_R^2 f_D - \ddot{\nu})\,\mathrm{d}s. \tag{3}$$

The nondimensional variables are defined by

$$x = \frac{X}{L}, \quad y = \frac{Y}{L}, \quad w = \frac{W}{L}, \quad \nu = \frac{V}{L}, \quad s = \frac{S}{L}, \quad l_0 = \frac{L_0}{L},$$

$$\tau = \frac{t}{\sqrt{\rho_P h L^4/D}}, \quad \alpha = \frac{a}{\sqrt{\rho_P h L^4/D}}, \quad f^\star = f\sqrt{\rho_P h L^4/D},$$

$$f_L = \frac{F_L}{\rho_F U^2}, \quad f_D = \frac{F_D}{\rho_F U^2}, \tag{4}$$

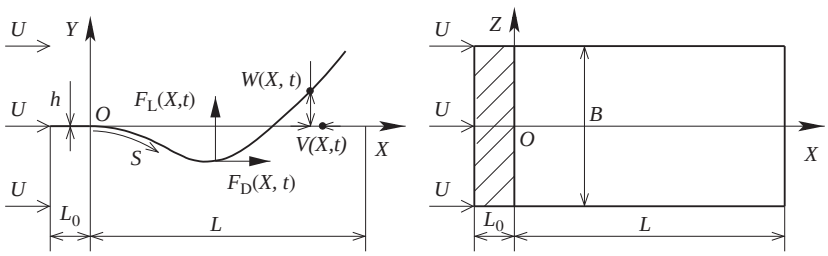

Fig. 1. Two orthogonal views of a cantilevered flexible in axial flow, and definitions of various quantities used in the paper.

where $f^\star$ and f are, respectively, nondimensional and dimensional vibration frequencies. Moreover, the mass ratio μ and reduced flow velocity U_R are, respectively, defined by

$$\mu = \frac{\rho_F L}{\rho_P h}, \quad U_R = UL\sqrt{\frac{\rho_P h}{D}}. \tag{5}$$

In Eqs. (1) and (3), the aero/hydrodynamic loads are calculated using the unsteady lumped vortex model [15]. On each individual panel, the pressure difference across the plate Δp is first computed and then decomposed into the *lift* f_L and the *drag* f_D. That is

$$f_{Li} = \Delta p_i \cos\alpha_i, \quad f_{Di} = \Delta p_i \sin\alpha_i + C_D, \tag{6}$$

where α_i is the angle of incidence of the ith panel. In the second equation above, an additional drag coefficient C_D may be considered, uniformly distributed over the whole length of the plate, to account for viscous drag effects. It should be motioned that $C_D = 0$ is used in the present paper for simplicity; the influence of this parameter, which is small, on the dynamics of cantilevered flexible plate in axial flow has been studied in Ref. [15].

It follows from Eq. (1) that the nondimensional power $P_{Fi}^\star$ of the work done by the transverse fluid load f_{Li} on the ith panel, in the sense of per unit length along the spanwise dimension of the plate, can be calculated from

$$P_{Fi}^\star = [f_{Li}\Delta s]\dot{w}(s_i), \tag{7}$$

and the nondimensional *accumulated* work $W_{F_i}^\star$ on the ith panel from

$$W_{F_i}^\star = \int_0^\tau [f_L \Delta s]\dot{w}(s_i)\,\mathrm{d}\tau. \tag{8}$$

Therefore, over the whole length of the plate, the nondimensional total power $\widehat{P}_F^\star$ and the nondimensional accumulated total work $\widehat{W}_F^\star$ can, respectively, be calculated by

$$\widehat{P}_F^\star = \sum_{i=1}^{N} P_{Fi}^\star, \quad \widehat{W}_F^\star = \sum_{i=1}^{N} W_{F_i}^\star, \tag{9}$$

where N is the number of panels considered in the aero/hydrodynamic model.

It is noted that $\widehat{W}_F^\star$ is the time integral of the power $\widehat{P}_F^\star$. When the plate flutters, $\widehat{P}_F^\star$ also oscillates about zero, as shown in Fig. 2(a); that is, in a vibration cycle of the plate, f_L does both positive work (the energy transferred from the fluid to the plate) and negative work (the energy transferred from the plate to the fluid). Since $\widehat{P}_F^\star$ oscillates, the plot of $\widehat{W}_F^\star$ versus time is not smooth, as one can see in Fig. 2(b). The oscillating $\widehat{P}_F^\star$ may be evaluated in terms of the time-averaged power $\overline{P}_F^\star$, for example, which is the time-averaged power in a vibration cycle of the system. In this paper, as illustrated in the inset of Fig. 2(b), we conveniently use the slope of the $\widehat{W}_F^\star$ versus time plot, in terms of the line connecting the local maxima (or local minima), to calculate $\overline{P}_F^\star$. Moreover, according to the nondimensionalization schemedefined in Eqs. (4), the dimensional time-averaged power $\overline{P}_F$ can be calculated by

$$\overline{P}_F = \rho_F U^2 \sqrt{\frac{D}{\rho_P h}}\overline{P}_F^\star. \tag{10}$$

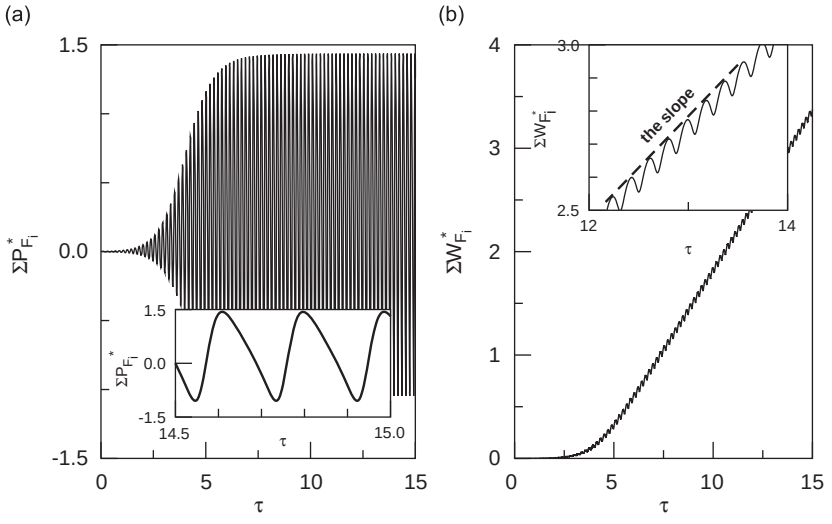

Fig. 2. (a) The power of the work done by the fluid load f_L; (b) the accumulated work done by f_L and the calculation of time-averaged power $\overline{P}_F^\star$. The parameters of the system are: $\mu = 0.2$, $U_R = 10.95$, $l_0 = 0.01$, $\alpha = 0.004$ and $C_D = 0$.

The Galerkin method is used in the solution of the equation of motion of the plate [15], and the vibration velocity of the plate $\dot{w}(s_i,\tau)$ can be expanded in terms of the velocity associated with generalized coordinate $\dot{q}_m$ and the beam mode ϕ_m as

$$\dot{w}(s_i,\tau)=\sum_{m=1}^{M}\dot{q}_m(\tau)\phi_m(s_i), \tag{11}$$

where M is the number of modes considered in the analysis. Therefore, one can calculate the (cumulative) total work $\Psi^{\star}_{\mathrm{F}_m}$ done by f_{L} in terms of each individual beam mode ϕ_m, defined by

$$\Psi^{\star}_{\mathrm{F}_m}=\sum_{i=1}^{N}\int_0^{\tau} f_{\mathrm{L}}\Delta s\dot{q}_m(\tau)\phi_m(s_i)\,\mathrm{d}\tau. \tag{12}$$

It should be noted that, no matter how one evaluates the energy transfer between the plate and the surrounding fluid flow, in terms of various locations along the length of the plate or various vibration modes, the total work done by the fluid is the same, i.e., $\widehat{W}^{\star}_{\mathrm{F}}=\sum_{i=1}^{N}W^{\star}_{\mathrm{F}_i}=\sum_{m=1}^{M}\Psi^{\star}_{\mathrm{F}_m}$.

Another issue that should be made clear is the determination of the point s_i. In this paper, s_i is chosen at the collocation point of the ith panel. That is, for example, when the number of panels is $N=200$ in the numerical simulation and the energy transfer at location $s_i=0.7$ is considered, we actually calculate all the quantities relating to the fluid load, the motion of the plate, the work and the power at the collocation point of the 140th panel.

3. Energy transfer

The objective of this section, dealing with energy transfer between the fluid flow and the plate, is two-fold: (i) to study the mechanism underlying the instability of the fluid–structure interaction system through energy analyses and (ii) to provide basic information for the design of flutter-mill. When the stability threshold is exceeded and flutter takes place, energy is continuously pumped into the plate from the surrounding fluid flow for sustaining the flutter motion. Actually, this net gain of energy is used as an indication of the onset of flutter by Païdoussis [17] and Balint and Lucey [18]. The contributions of the present paper are that, for the first time, a breakdown of the total energy transfer between the fluid flow and the plate in different segments along the length of the plate and in different modes of the flutter motion is given; it should be emphasized that the energy analyses conducted in this manner provide vital information to a practical design of the flutter-mill.

3.1. Energy transfer at various values of U_{R}

The energy transfer between the cantilevered flexible plate and the fluid flow is first examined at various values of reduced flow velocity U_{R} in Fig. 3. For a specific system with parameters $\mu=0.2$, $l_0=0.01$, $\alpha=0.004$ and $C_{\mathrm{D}}=0$, the dynamics is discussed in detail in [15]; the critical point of the system is at $U_{\mathrm{Rc}}=9.925$. When $U_{\mathrm{R}}<U_{\mathrm{Rc}}$, any disturbance to the system dies down with time and the plate always returns to the static flat state. However, as one can see in Fig. 3(a), when $U_{\mathrm{R}}=9.823=0.99U_{\mathrm{Rc}}$, the total work $\widehat{W}^{\star}_{\mathrm{F}}$ is positive; the positive work done by the fluid on the plate is consumed by dissipation within the plate: the material damping and the nonconservative aero/hydrodynamic drag (f_{D}). As time elapses, the vibration amplitude of the system decreases and the increase of $\widehat{W}^{\star}_{\mathrm{F}}$ gradually saturates; that is, the power $\widehat{P}^{\star}_{\mathrm{F}}$ (or the time derivative of $\widehat{W}^{\star}_{\mathrm{F}}$) approaches zero. It is found that when U_{R} is well below U_{Rc}, say $U_{\mathrm{R}}=8.660=0.873U_{\mathrm{Rc}}$, $\widehat{W}^{\star}_{\mathrm{F}}$ is still positive. Nevertheless, when U_{R} is very low, as is the case for$U_{\mathrm{R}}=7.756=0.781U_{\mathrm{Rc}}$ shown in Fig. 3(a), $\widehat{W}^{\star}_{\mathrm{F}}$ becomes negative; that is, the effect of the fluid load f_{L}, which *purely* resists the motions of the plate in this case, is equivalent to an additional damping mechanism.

When $U_{\mathrm{R}}>U_{\mathrm{Rc}}$, flutter takes place. It can be seen in Fig. 3(b) for $U_{\mathrm{R}}=10=1.008U_{\mathrm{Rc}}$ that $\widehat{W}^{\star}_{\mathrm{F}}$ is positive and its value continuously grows, as compared to the case $U_{\mathrm{R}}=9.823$ shown in Fig. 3(a). Moreover, as shown in Fig. 3(c), with increasing U_{R}, the flutter amplitude of the system increases, and more work is done by f_{L}. It is of interest to examine the slope of the $\widehat{W}^{\star}_{\mathrm{F}}$ versus time plots (i.e., the values of $\overline{P}^{\star}_{\mathrm{F}}$) presented in Figs. 3(b) and (c) for the cases $U_{\mathrm{R}}>U_{\mathrm{Rc}}$. One finds that, at a fixed value of U_{R}, as the flutter amplitude grows with time, $\overline{P}^{\star}_{\mathrm{F}}$ continuously increases; when limit cycle oscillations are attained, $\overline{P}^{\star}_{\mathrm{F}}$ becomes a constant. This observation reveals that, as the flutter amplitude is increased, more energy is pumped into the plate from the fluid flow; at the same time, more energy is dissipated by the plate. Nevertheless, in the end, a balance between input energy and dissipation in the plate can be attained, and thus a constant flutter amplitude of the stable limit cycle oscillations. Moreover, with increasing U_{R}, the flutter amplitude grows, so does the value of $\overline{P}^{\star}_{\mathrm{F}}$; that is, at higher U_{R}, the balance between input energy and dissipation is attained at a higher level of energy transfer between the plate and the fluid flow.

It should be mentioned that an unresolved problem in the study of cantilevered flexible plates in axial flow is that in experiments [19–23] a subcritical onset of flutter was frequently observed, as well as considerable hysteresis, while all theories to date, including the one in the present paper, have predicted only a supercritical onset of flutter. In Ref. [15], Tang and Païdoussis discussed this discrepancy between experiments and theories; one of the possible explanations may be that it is a viscous effect associated with boundary-layer and/or flow separation, not modelled in all theories. It can be observed

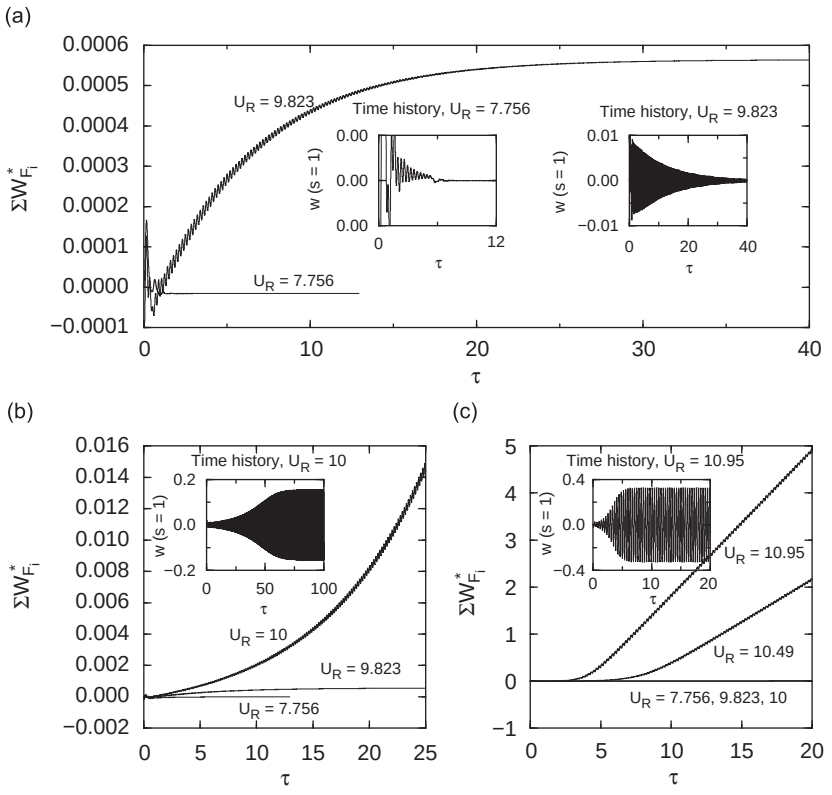

Fig. 3. The work, $\widehat{W}^{\star}_{F} = \sum_{i=1}^{N} W^{\star}_{F_i}$, done by the fluid load f_L at various values of U_R: (a) for $U_R = 7.756$ and 9.823; (b) for $U_R = 10$ ($U_R = 7.756$ and 9.823 are also shown for comparison); (c) for $U_R = 10.49$ and 10.95 ($U_R = 7.756$, 9.823 and 10 are also shown for comparison). The other parameters of the system are: $\mu = 0.2$, $l_0 = 0.01$, $\alpha = 0.004$ and $C_D = 0$.

clearly in the experiments conducted by Zhang et al. [19] that the onset of flutter is accompanied by the evolution of the vortical wake from a von Kármán type to an undulating one. That is, as indicated by the two different types of wake before and after the onset of flutter, the patterns of the boundary-layer and/or flow separation may be different. Note that, in the latter case, there are dynamical interactions between the flow and the plate. Therefore, one can reasonably conjecture that, from the viewpoint of energy analysis, more energy than models predict is required by the plate to flutter from the static flat state. In other words, the boundary-layer and/or flow separation before the onset of flutter (with a von Kármán type wake as the indication) acts effectively as a energy-barrier and delays the onset of flutter. On the other hand, when the plate flutters, less energy is dissipated into the (undulating) vortical wake and thus the plate would resume stable state at a lower flow velocity.

3.2. Energy transfer at various locations of the plate

It has been shown in [15] that the vibration modes of a cantilevered flexible plate in axial flow are strongly dependent on the mass ratio μ of the system. Additionally, it has been found that points at different locations along the plate do not oscillate in phase (as some parts of the plate move upwards, others move downwards). Therefore, it is of interest to examine the energy transfer between the plate and the fluid flow at various locations along the plate for various cases of μ.

As shown in Fig. 4 for a specific system with parameters given in the figure caption ($\mu = 0.2$, $U_R = 10.95 = 1.103U_{Rc}$), the energy transfer at various locations is not the same: energy is pumped from the fluid flow into the plate (positive slope of the $W^{\star}_{F_i}$ versus time plot) at some locations; while it is transferred from the plate to the fluid flow (negative slope) at other locations. In particular, $W^{\star}_{F_i}$ is positive at points $s_i = 0.025$–0.675; while, it is negative at points $s_i = 0.750$–1. Note that in this case, the total work done by the fluid load f_L, i.e., the sum of all $W^{\star}_{F_i}$ along the whole length of the plate, $\widehat{W}^{\star}_{F} = \sum_{i=1}^{N} W^{\star}_{F_i}$, is positive, as shown in Fig. 4(d). The important finding is that, as energy is pumped into the plate at the upstream segment of the plate, it is transferred from the plate to the fluid flow at the downstream segment.

The distribution of the positive/negative $W^{\star}_{F_i}$ depends on the value of U_R. As shown in Fig. 5, for a smaller reduced flow velocity, $U_R = 10 = 1.008U_{Rc}$ (the other parameters, especially the mass ratio μ, are the same as those in Fig. 4), for which $\widehat{W}^{\star}_{F}$ is still positive, $W^{\star}_{F_i}$ is negative at points $s_i = 0.025$–0.175, positive in the range $0.2 \le s_i \le 0.75$ and negative at points $0.775 \le s_i \le 1$; note that the energy is still transferred from the plate to the fluid flow in the downstream segment of the plate.

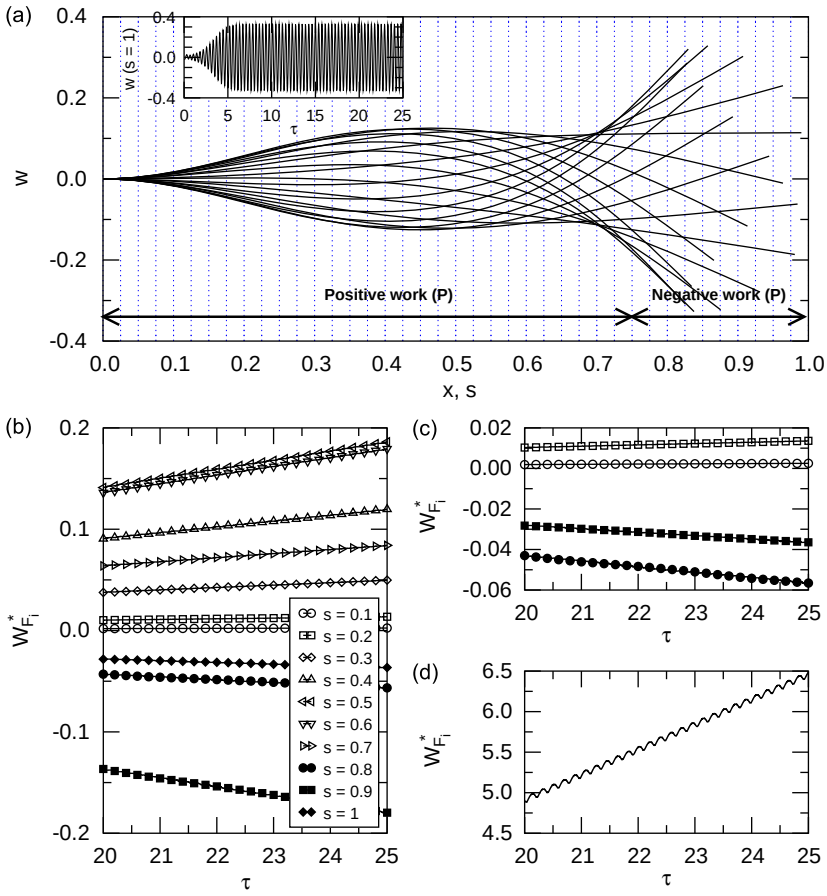

Fig. 4. The energy exchange between the cantilevered flexible plate and the surrounding fluid flow along the length of the plate: (a) the flutter modes; (b) the work done by f_L at various locations; (c) an enlargement of part of (b); (d) the total work done by f_L. The system parameters used are: $\mu = 0.2$, $U_R = 10.95\,(= 1.103U_{R_c})$, $l_0 = 0.01$, $\alpha = 0.004$ and $C_D = 0$. Note that $N = 200$ panels are used in the numerical simulation. The energy transfer at 40 locations (every five panels) is recorded and the results at 10 locations (every 20 panels) are presented.

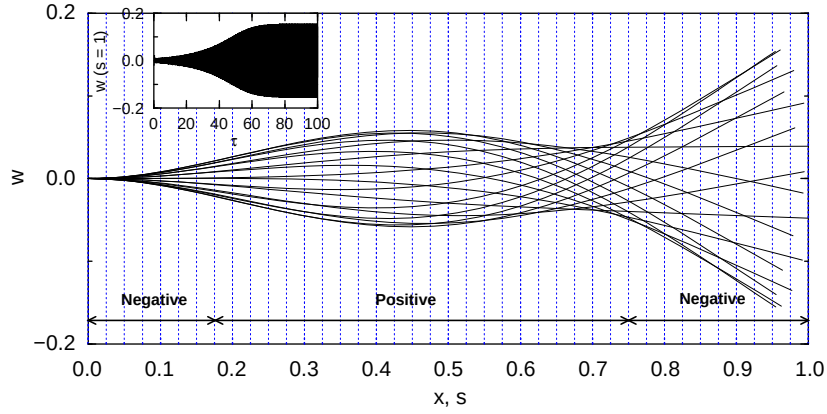

Fig. 5. The positive/negative work done by the fluid load f_L at various locations along the length of the plate. The parameters of the system are: $\mu = 0.2$, $U_R = 10$, $l_0 = 0.01$, $\alpha = 0.004$ and $C_D = 0$. Note that $N = 200$ panels are used in the numerical simulation. The energy transfer at 40 locations (every five panels) is recorded.

An important remark should be made here. Superficially, the finding that energy is lost to the plate in the downstream part may appear to contradict the findings of Benjamin [24], Gregory and Païdoussis [25], and Païdoussis [17] for a pipe conveying fluid, namely that, for positive work to be done on the plate, the free-end slope and velocity must be in

quadrature; i.e., when the slope is negative, the velocity of the free end of the pipe must be positive, and vice versa. Thus, emphasis is placed on the free end, while here we have shown that the downstream end of the plate loses energy uniformly. On closer examination, however, what Benjamin [24] have found is (i) that positive work is done on the system (energy is transferred from the fluid to the structure) where there is a curvature, which is in the middle of the structure for basically second-beam-mode flutter, (ii) at the downstream end, Coriolis forces dominate, resulting in energy loss, and (iii) the second-beam-mode motion results in the quadrature relationship between slope and velocity at the free end. Thus, there is no contradiction in the basic energy transfer mechanism found here for the plate and that for the pipe, as well as that for a cylinder in axial flow [26].

The distribution of the positive/negative $W^{\star}_{\mathrm{F}_i}$ is also examined for various systems with different values of μ, as shown in Fig. 6. It should be mentioned that different values of U_{R} are used for individual cases of μ for the purpose of obtaining flutter motions; as shown in Table 1, for each case of μ, U_{R} is so chosen that it is about 10% above the corresponding critical point $U_{\mathrm{R_C}}$. It can be seen in Fig. 6 that the distribution of the positive/negative $W^{\star}_{\mathrm{F}_i}$ depends on μ. When μ is large, say $\mu = 2$

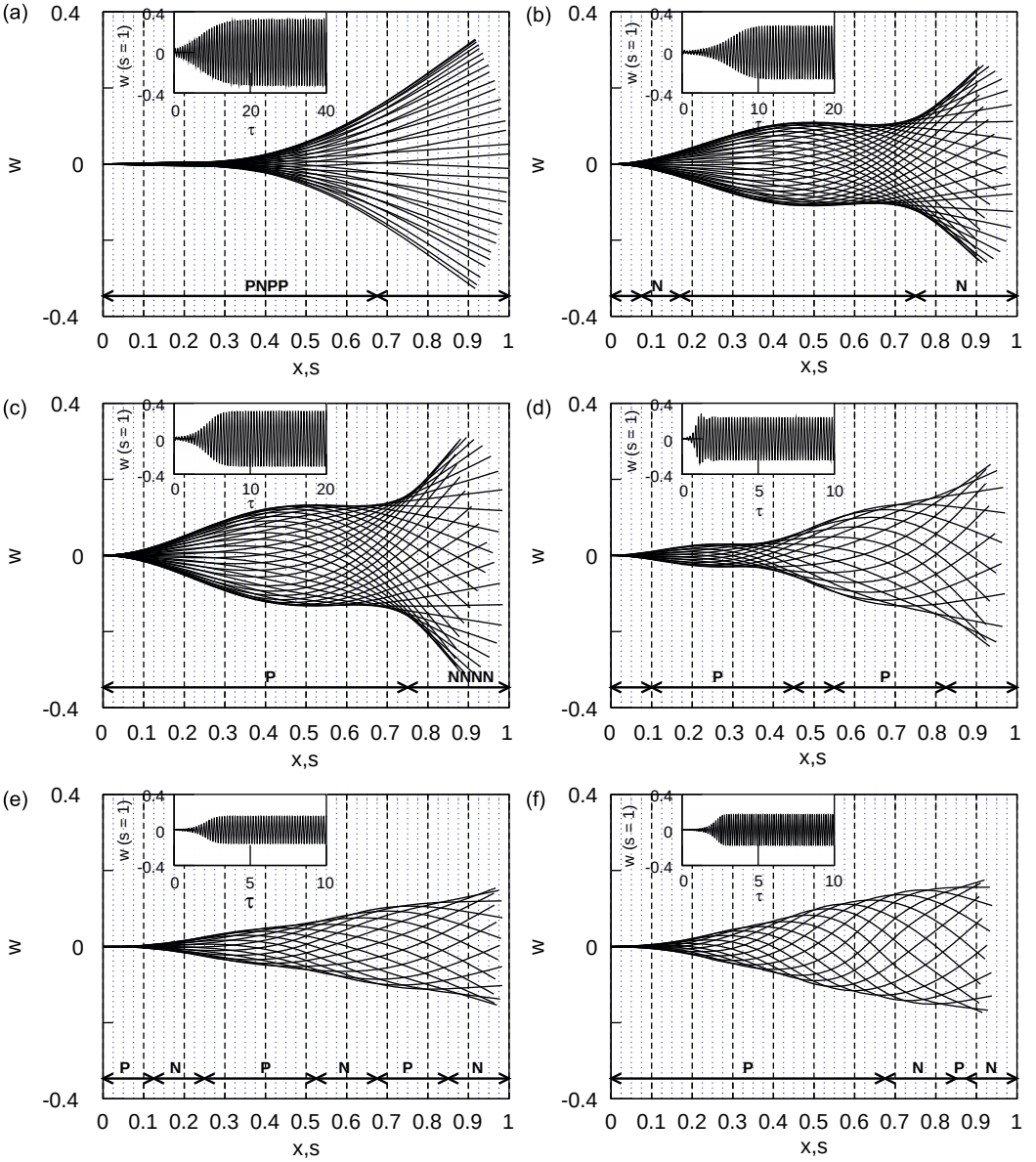

Fig. 6. When flutter takes place, the positive/negative (P/N) work done by the fluid load f_{L} at various locations along the length of the plate: (a) $\mu = 0.01$, $U_{\mathrm{R}} = 40.62$, (b) $\mu = 0.5$, $U_{\mathrm{R}} = 7.483$, (c) $\mu = 0.5$, $U_{\mathrm{R}} = 7.746$, (d) $\mu = 2$, $U_{\mathrm{R}} = 11.83$, (e) $\mu = 5$, $U_{\mathrm{R}} = 11.40$, and (f) $\mu = 20$, $U_{\mathrm{R}} = 9.478$. The other parameters of the system are: $l_0 = 0.01$, $\alpha = 0.004$ and $C_{\mathrm{D}} = 0$. Note that, the number of panels $N = 200$ is used for the cases $\mu = 0.01$ and 0.5; while, for the other cases ($\mu = 2$, 5 and 20), $N = 400$ is used. The energy transfer at 40 locations (every five panels in the case of $N = 200$ and every 10 panels when $N = 400$) are recorded.

Table 1
The reduced flow velocities U_R used in the examination of energy transfer of various systems with different values of mass ratio μ (see Fig. 6).

μ	0.01	0.5	0.5	2	5	20
U_{Rc}	37.08	6.9	6.9	10.78	10.51	8.709
U_R	40.62	7.483	7.746	11.83	11.40	9.487
$(U_R - U_{Rc})/U_{Rc}$ (%)	9.55	8.45	12.26	9.76	8.47	8.17

or 5, higher modes become important in the dynamics of the system [15], and the distribution of positive/negative $W^{\star}_{F_i}$ has a complicated pattern: many changes between N (negative) and P (positive). However, when $\mu = 20$, it seems that the pattern of the distribution of positive/negative $W^{\star}_{F_i}$ does not have as many alternations in sign as the cases $\mu = 2$ and 5. Finally, one can see in Fig. 6 that, no matter what values of μ and U_R are used, energy is transferred from the plate to the fluid flow at the most downstream section of the plate (N in the figure).

In the present section, the energy transfer between the fluid flow and the plate has been studied at various locations along the length of the plate. It has been shown that positive/negative parts, in terms of the work done by the fluid on the plate, alternately occur along on the plate. The distribution pattern of positive/negative work is found to be dependent on the value of mass ratio μ, and energy is always transferred from the plate to the fluid flow at the most downstream section of the plate. These findings are by no means trivial: they are closely correlated to the design of flutter-mill, as discussed later in the present paper; moreover, they may give new insights into the propulsion mechanism of oscillating foils, as done in the next paragraph parenthetically.

Evident similarities in the oscillation modes can be seen between the plates in the current stability problem and fish in anguilliform swimming, say for an eel (*anguilla vulgaris*, see [27, Fig. 4]).[1] Fish propulsion has frequently been studied by means of rigid or flexible foils undergoing active motions with prescribed kinematics in fluid flow [28,29]; generation of thrust and propulsion efficiency are the major concerns. No previous work has ever answered the question as to which body segments and to what extent a fish is inherently flexible and undergoes deformations in a more passive manner under the hydrodynamic loads, and which parts and to what extent a fish becomes effectively more rigid and does work on the fluid. Although there is no doubt that energy has to be transferred from the fish to the surrounding fluid to generate locomotion, details of the energy transfer between the fish and the fluid flow, in conjunction with the swimming mode adopted (where the mass ratio μ is an important parameter), will provide valuable information for a better understanding of the propulsion mechanism as well as a better design of a swimming robot. To this end, the findings in the current stability problem, to be roughly regarded as an inverse one of the propulsion problem, suggest that energy transfer in different directions can occur along the body of a fish, and that the rear segment of the fish always contributes to the overall locomotion (does positive work on the fluid).

3.3. Energy transfer in terms of individual beam modes

As the Galerkin method is used in the solution of the governing equations of the plate [15], it is convenient to examine the energy transfer between the plate and the fluid flow in terms of individual beam modes. Additionally, one can find that the investigations in this section are directly related to the design of flutter-mill discussed later in the present paper.

In Fig. 7, the work done by the fluid load f_L at various values of U_R for a specific system with $\mu = 0.2$ is studied. It can be seen that, at all values of U_R (cf. Fig. 3), the energy transfer between the plate and the fluid flow occurs largely in the first two beam modes, ϕ_1 and ϕ_2 (note that the plate vibrates in the second beam mode when $\mu = 0.2$; see [15] and Figs. 4(a) and 5 of the present paper); the magnitudes of $\Psi^{\star}_{F_{m,m\geq 3}}$ are much smaller than those of $\Psi^{\star}_{F_{m,m=1,2}}$. Moreover, one finds that, at different values of U_R, the work done by f_L in terms of ϕ_2 is *always* positive, while for $\Psi^{\star}_{F_{m,m\neq 2}}$ it may be either positive or negative.

As shown in Fig. 7(a.1), for the case $U_R = 7.756 = 0.781U_{Rc}$, where $\sum_{m=1}^{M}\Psi^{\star}_{F_m}$ is negative (see Fig. 3(a)), $\Psi^{\star}_{F_1}$ is negative and $\Psi^{\star}_{F_2}$ is positive; moreover, the magnitude of $\Psi^{\star}_{F_1}$ is larger than that of $\Psi^{\star}_{F_2}$. That is, when energy is pumped into the plate in the second beam mode, more energy is transferred from the plate to the fluid flow in the first beam mode. It should be mentioned that the plate is forced to be deformed in the first beam mode with a small amplitude at the starting point of the dynamics simulations, i.e., initial conditions $q^0_1 = -1.0\times 10^{-2}$, $q^0_{i,i\neq 1} = 0$ and $\dot{q}^0_i = 0$ are used; hence, at the beginning of the motions of the plate, there is some initial energy stored in the plate in the first beam mode. At relatively higher U_R, but still below the critical point U_{Rc}, for example for $U_R = 9.823 = 0.99U_{Rc}$ shown in Fig. 7(b.1), for which $\sum_{m=1}^{M}\Psi^{\star}_{F_m}$ becomes positive (see Fig. 3(a)), $\Psi^{\star}_{F_1}$ is still negative. However, when $U_R > U_{Rc}$, $\Psi^{\star}_{F_1}$ becomes positive, as shown in Fig. 7(c.1), energy is transferred from the fluid flow to the plate in terms of both ϕ_1 and ϕ_2. For higher U_R, as one can see in Figs. 7(d.1) and (e.1), $\Psi^{\star}_{F_1}$ remains positive; moreover, both slopes of the $\Psi^{\star}_{F_1}$ and $\Psi^{\star}_{F_2}$ versus time plots increase.

[1] We here limit our discussions to anguilliform locomotion because the three-dimensional flow pattern and the vortex interactions between the posterior part of a fish body and its caudal fin become important in other swimming modes such as carangiform and thunniform propulsion, and the theoretical model would be significantly different from that of a rectangular plate model in fluid flow.

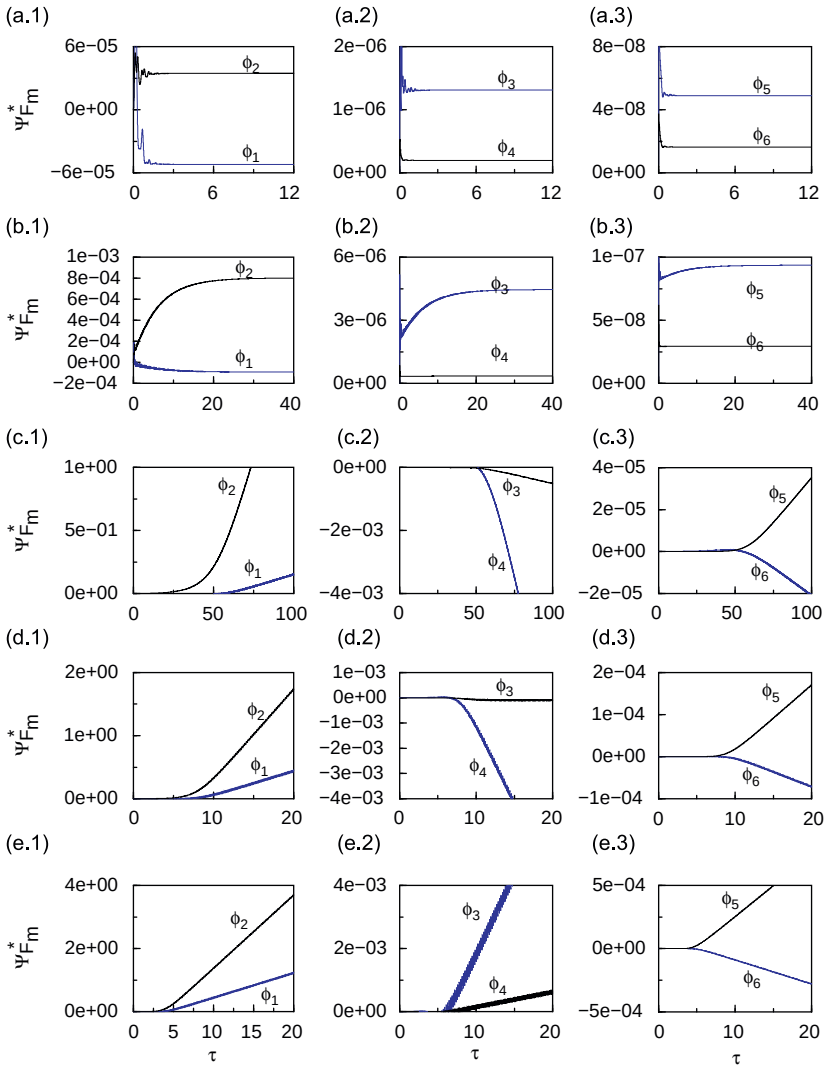

Fig. 7. The work done by the fluid load f_L in terms of individual beam modes. The mass ratio of the system is $\mu = 0.2$ and various values of U_R are examined: (a.1)–(a.3) $U_R = 7.756$, (b.1)–(b.3) $U_R = 9.823$, (c.1)–(c.3) $U_R = 10$, (d.1)–(d.3) $U_R = 10.49$, and (e.1)–(e.3) $U_R = 10.95$. The other parameters of the system are: $l_0 = 0.01$, $\alpha = 0.004$ and $C_D = 0$. Note that $M = 12$ modes are used in the numerical simulation, and only the results of the first six are presented.

The energy transfer between the plate and the fluid flow in terms of individual beam modes is also studied for systems with other values of mass ratio μ, as shown in Fig. 8. Again, different values U_R are used for individual cases of μ in order to examine the energy transfer in the fluttering plate; the values of U_R used are listed in Table 1. It can be seen in Fig. 8 that, when μ is small, say $\mu = 0.01$ or 0.5, the energy transfer occurs largely in the first two beam modes ϕ_1 and ϕ_2, while, when μ is large, as for $\mu = 2$, 5 and 20, the magnitudes of the work done by f_L in higher beam modes become comparable with, or even larger than, those for ϕ_1 and ϕ_2. For example, as shown in Figs. 8(e.1) and (e.2) for the case $\mu = 20$ and $U_R = 9.487$, one finds that $|\Psi^{\star}_{F3,4}| > |\Psi^{\star}_{F1,2}|$.

4. The flutter-mill

It has been shown that, over the whole length of the plate and in the time-averaged sense, energy is indeed pumped into the plate from the fluid flow when flutter takes place. We can therefore utilize the energy extracted from the fluid flow to do useful work; for example, as shown in Fig. 9, in the design of a flutter-mill to generate electricity.

As illustrated in Fig. 9(a), a plate made of flexible material with embedded conductors is placed between two parallel magnetic panels. When flutter takes place, the motion of each conductor in the magnetic field generates an electric potential difference between its upstream and downstream ends; and the wiring scheme shown in Fig. 9(b) ensures the

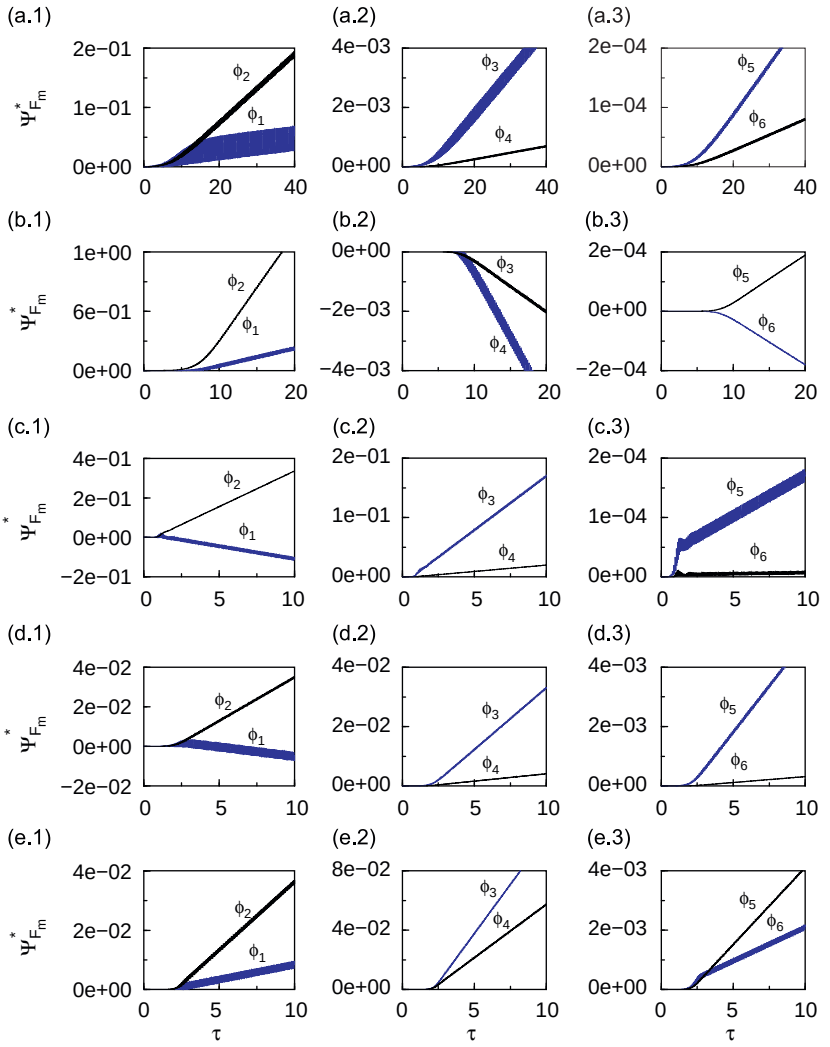

Fig. 8. The work done by the fluid load f_L in terms of individual beam modes; various cases of the mass ratio μ are examined: (a.1)–(a.3) $\mu = 0.01$, $U_R = 40.62$, (b.1)–(b.3) $\mu = 0.5$, $U_R = 7.483$, (c.1)–(c.3) $\mu = 2$, $U_R = 11.83$, (d.1)–(d.3) $\mu = 5$, $U_R = 11.40$, and (e.1)–(e.3) $\mu = 20$, $U_R = 9.478$. The other parameters of the system are: $l_0 = 0.01$, $\alpha = 0.004$ and $C_D = 0$. Note that $M = 12$ modes are used in the numerical simulation, and only the results of the first six are presented.

formation of a closed circuit to supply electrical power to the load, say a rechargeable battery. The rigid bars and the spring supports shown in Fig. 9 are taken into consideration to make the design more realistic and/or to improve the performance of the device, for example to reduce the flutter threshold. The influence of an additional spring support and a concentrated mass (i.e., the rigid bar) on the system dynamics has been studied in another paper by Tang et al. [30].

For the present, we do not consider a plate made of piezoelectric material [10,11,31] in the design because deformation of a *cantilevered* plate normally induces very low strain levels, and the induced electrical potential would thus be small. Moreover, although an advanced piezoelectric material may generate high electrical potential, the low accompanying electric current seriously limits the power output. Nevertheless, the possibility of a piezoelectric plate for the flutter-mill deserves further examination in the future.

As quite a few of parameters are involved in the dynamics of cantilevered flexible plates in axial flow [15] as well as in the energy transfer between the plate and the surrounding fluid flow, a starting point should be chosen for a conceptual design. We first recall that, at different segments of the plate, the energy transfer may be from the fluid flow to the plate or vice versa. Therefore, the conductors embedded in the flexible plate should correspondingly be arranged in several segments, or say phases. Too many phases of conductor arrangement lead to difficulties in the design of the wiring scheme and the rectifier. To this end, in the light of the vibration modes of the system for various values of mass ratio μ (see [15, Fig. 12] and also Figs. 4–8 of the present paper), we consider a system with $\mu < 1$, for which the plate vibrates in the second beam mode and the energy transfer largely occurs in the first two beam modes; hence, only two phases of

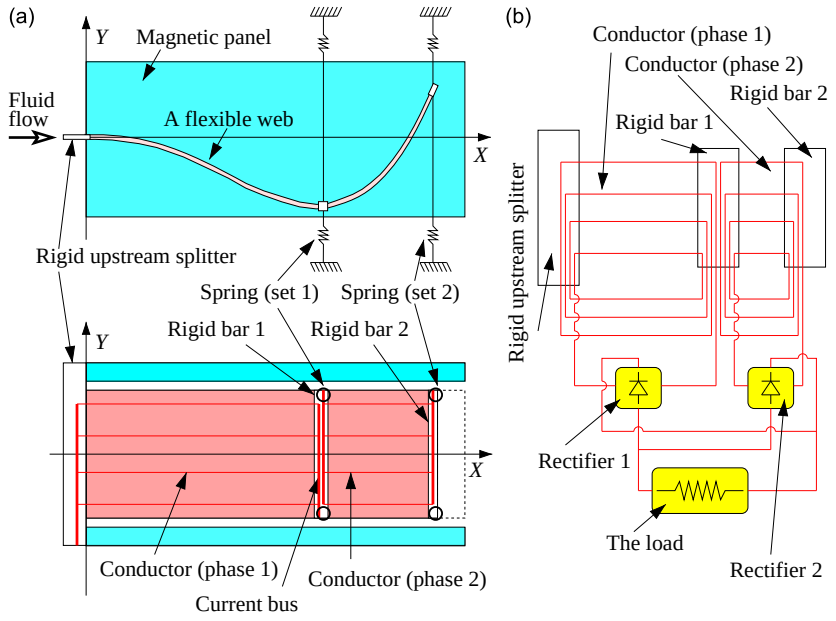

Fig. 9. The conceptual design of a flutter-mill: (a) layout of the system and (b) the wiring scheme.

Table 2
Design data of a cantilevered flexible plate in axial flow with the mass ratio $\mu = 0.5$ or 0.2.

Parameters	Plate 1 ($\mu = 0.5$)	Plate 2 ($\mu = 0.2$)	Units
Physical parameters			
ρ_F	1.226	1.226	kg/m^3
ρ_P (Al-7505)	2840	2840	kg/m^3
h	0.0005	0.0005	m
E	7.056×10^{10}	7.056×10^{10}	Pa
v	0.3	0.3	
a	0.0005	0.0005	s
B	(0.2 used)	(0.2 used)	m
L (varied in design)	0.58	0.232	m
L_0 (varied in design)	0.0058	0.0023	m
Nondimensional parameters excepting μ and U_R			
$l_0 = L_0/L$	0.01	0.01	
$\alpha = a/\sqrt{\rho_P h L^4/D}$	0.001 (0.004 used)	0.070 (0.004 used)	
C_D	(0 used)	(0 used)	

conductor arrangement are necessary. It should be mentioned that, no matter whether it is transferred from the fluid flow to the plate in some segments of the plate or vice versa elsewhere, the energy ultimately comes from the fluid flow.

In the present paper, we primarily consider two cases: $\mu = 0.5$ and 0.2. In the conceptual design of flutter-mill, dimensional parameters may allow one to evaluate the performance of the device in a more direct manner; to this end, we consider a plate made of aluminium in axial air flow [21]. The reason for a metallic plate is that metal conductors are supposed to be embedded in a plate, otherwise made of a very flexible material; the properties of this *composite* plate would be largely determined by those of the conductors. The parameters of the two systems with $\mu = 0.5$ and 0.2 are listed in Table 2.

Some explanation is necessary for the data in Table 2. Firstly, since nondimensional parameters are used in all numerical simulations, the physical parameters of the systems listed in Table 2 are actually obtained using a reverse approach: for an aluminium plate in axial air flow, we know the properties of the fluid and the plate material; the thickness of the plate h is determined as $h = 0.5$ mm and then the length of the plate can be calculated for the case $\mu = 0.5$ or 0.2. Secondly, the nondimensional parameters $l_0 = 0.01$, $\alpha = 0.004$ and $C_D = 0$ are uniformly used; the influence of these parameters on the dynamics of the system have already been discussed [15]. It should be noted that, as the same material is considered, the loss factor a for both $\mu = 0.5$ and 0.2 should be the same. However, the nondimensional material damping coefficient α

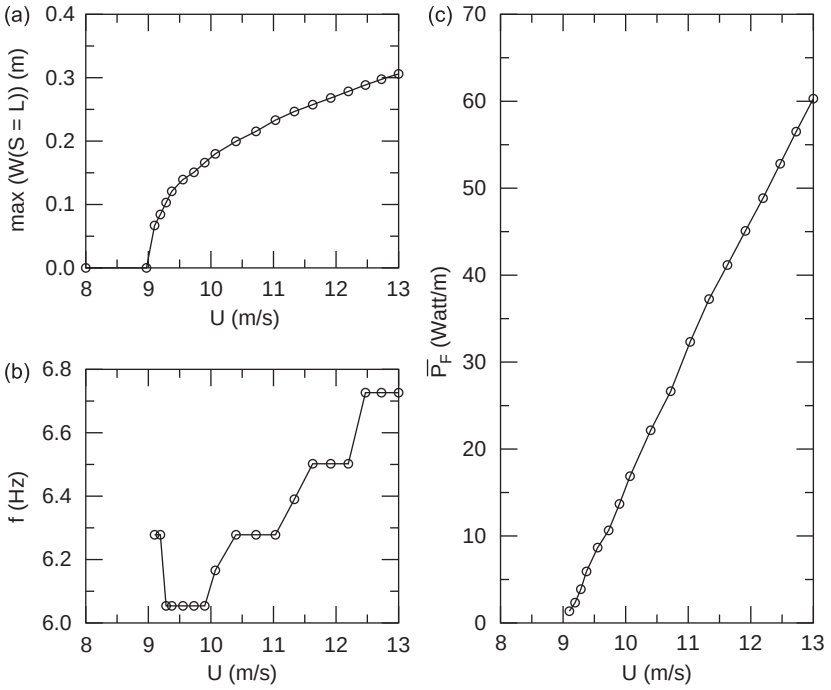

Fig. 10. The dynamics of the system with $\mu = 0.5$ and the time-averaged power $\overline{P}_F$ of the fluid load f_L: (a) the bifurcation diagram; (b) the flutter frequency; (c) the time-averaged power $\overline{P}_F$. The other parameters of the system are: $l_0 = 0.01$, $\alpha = 0.004$ and $C_D = 0$.

depends on the length of the plate L, and the values for the cases $\mu = 0.5$ and 0.2 are different. Therefore, when we use the uniform value $\alpha = 0.004$ in the numerical simulations, the value of α is overvalued for the case $\mu = 0.5$ and undervalued for $\mu = 0.2$. It has been shown [15] that a larger value of α results in a higher critical point U_{Rc}; that is, at a fixed U_R beyond U_{Rc}, the flutter amplitude (hence the level of energy transfer between the plate and the fluid flow) is underestimated for the case $\mu = 0.5$ and overestimated for $\mu = 0.2$. Thirdly, $B = 0.2$ m is considered in the conceptual design in order to avoid possible difficulties in attaining sufficient strength of the magnetic field between the two magnetic panels. It should be mentioned that the value of B is not used in the computation of the two-dimensional dynamics. Moreover, the choice of B does not affect the analysis of the energy transfer in terms of energy transfer/power density per unit length along the spanwise dimension of the plate. Finally, it has been found through numerical simulations [15] that the critical points for $\mu = 0.5$ and 0.2 are, respectively, $U_{Rc} = 6.899$ and 9.925; the corresponding dimensional flutter thresholds are, respectively, $U_c = 8.97$ and 32.27 m/s.

As shown in Figs. 10 and 11, preliminary calculations of the power extraction from the fluid flow demonstrate that the proposed flutter-mill is very promising for generation of electrical power. In particular, consider a design with mass ratio $\mu = 0.5$ and plate width $B = 0.2$ m; the device is compact, with overall dimensions length × width × height = 0.58 m × 0.2 m × 0.58 m, where the height is considered as twice the allowed maximum flutter amplitude (i.e., half of the length of the flexible plate). Such a system can be expected to extract 10 W power (at $U = 12$ m/s or 43.2 km/h) from the wind; and, if only 10% of the extracted wind energy is ultimately converted to the electrical power, an output of 1 W is guaranteed (which is the goal of energy-harvesting eel project [11]). Higher power output can be expected from the system with $\mu = 0.2$, which has even smaller overall dimensions (0.232 m × 0.2 m × 0.232 m) but works at higher flow velocities. Approximately, when $\mu = 0.2$, the power extraction is as high as $\overline{P}_F = 1$ kW/m at $U = 40$ m/s or 144 km/h.

We can compare the performance of the flutter-mill to a real HAWT, specifically the three-blade stall regulated turbine studied by Burton et al. [16], in terms of electrical power output, as shown in Fig. 12. The HAWT has a disk area 227 m^2 and the data for electrical power output are collected at the rotational speed 44 rpm. In order to make a comparison, we suppose that the flutter-mill has the same wind receiving area as the HAWT (227 m^2) and accordingly calculate the effective width B_{eff} of the plate; the desired width B_{eff} can be attained by considering an array of flutter-mills, each with a design width $B = 0.2$ m. Moreover, in the calculation of electrical power output, we assume that only 10% of the energy captured by the plate is ultimately converted to electrical power; the other 90% is consumed by the plate for sustaining the flutter motions (under the action of the induced electromagnetic forces). It can be seen in Fig. 12 that when $\mu = 0.5$, the flutter-mill works at the lower part of wind speed range of the HAWT; however, the flutter-mill electrical power output is not as high as that of the HAWT (about 10%). For the $\mu = 0.2$ design, the flutter-mill works at high wind speeds beyond the normal working conditions of the HAWT, but a very high electrical power output can be expected. Therefore, in principle, it

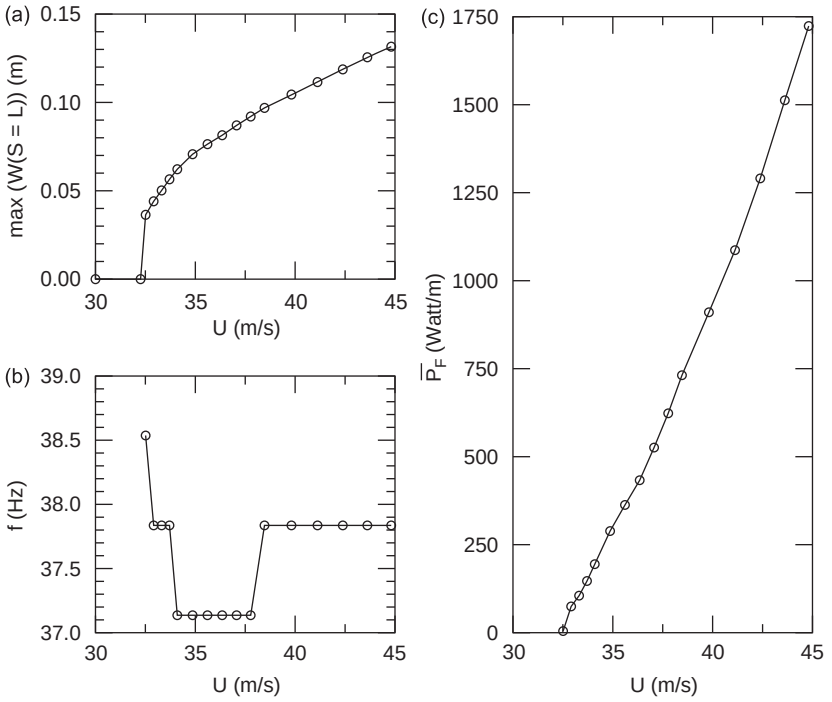

Fig. 11. The dynamics of the system with $\mu = 0.2$ and the time-averaged power $\overline{P}_F$ of the fluid load f_L: (a) the bifurcation diagram; (b) the flutter frequency; (c) the time-averaged power $\overline{P}_F$. The other parameters of the system are: $l_0 = 0.01$, $\alpha = 0.004$ and $C_D = 0$.

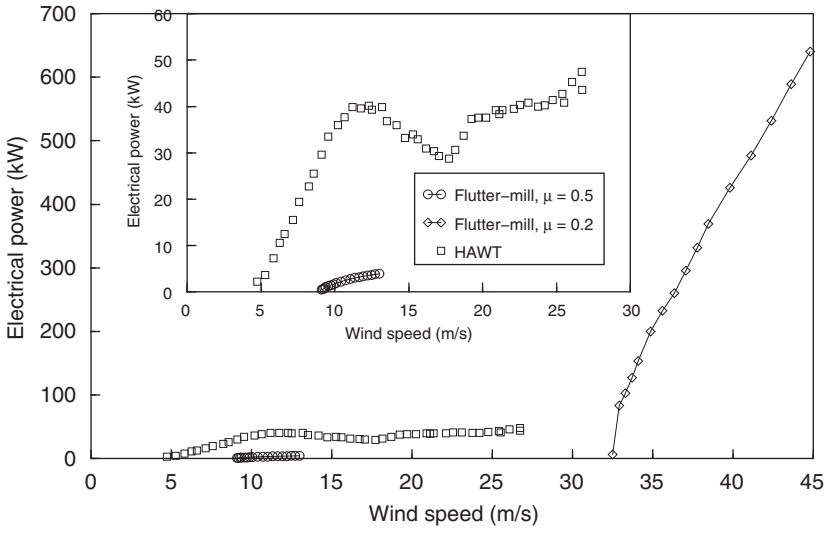

Fig. 12. The performance of the flutter-mill as compared to a real HAWT, i.e., the three-blade stall regulated turbine studied in [16].

is possible to design a flutter-mill with a mass ratio between $\mu = 0.2$ and 0.5 to achieve an output capacity comparable to the real HAWT and to operate in the same range of wind speeds.

It should be emphasized that the design of flutter-mill is still at a very preliminary stage. For example, it has been arbitrarily assumed in the present paper that 10% of the energy extracted by the device can be eventually converted into electrical power without taking into account the induced electromagnetic force acting on the plate. In fact, it is rather difficult to determine the induced electromagnetic force in the current model, because it not only depends on the dynamics of the plate but also the parameters of the magnetic field and the induced electrical current (and thus the electrical load). Additionally, other factors may be involved in the design, such as the springs and spanwise rigid bars illustrated in Fig. 9 have not been studied in the present paper in association with a specific design. However, as compared with previous concepts of turbineless electrical generators, one can find in this paper that the idea of flutter-mill is indeed based on

theoretical calculations, to the same extent as the wingmill [1,2,5–8] and the energy-harvesting eel [10,11], and better than the windbelt [13] and the hydro-generator with elastic oscillating wing [14]. Finally, it should be mentioned that a group at McGill University has started very recently to build a prototype of flutter-mill based on the findings presented in the present paper.

5. Conclusions

Cantilevered flexible plates in axial flow lose stability through flutter at sufficiently high flow velocity. In the present paper, the energy transfer between the plate and the surrounding fluid flow is studied, in terms of various locations along the length of the plate and various vibration modes of the system. Based on the energy analysis, a new energy-harvesting device utilizing the self-induced vibrations of a cantilevered thin flexible plate in axial flow is proposed. The performance of the flutter-mill is preliminarily evaluated, and key design parameters are determined according to the dynamics and energy transfer of the system. The power output capacity of two flutter-mills, with typical values of system parameters, is compared to a real HAWT. It is demonstrated that the flutter-mill can be designed to achieve high performance with compact size, and it is therefore very promising.

Acknowledgements

The leading author is supported by the Open Research Fund Program of Hubei Provincial Key Laboratory of Fluid Machinery and Power Engineering Equipment, and a Natural Sciences and Engineering Research Council of Canada (NSERC) Post-Doctoral Fellowship. The support of NSERC for this research is also gratefully acknowledged.

References

[1] D.A. Adamko, J.D. DeLaurier, An experimental study of an oscillating-wing windmill, in: *Proceedings of the Second Canadian Workshop on Wind Engineering*, 1978, pp. 64–66.
[2] W. McKinney, J.D. DeLaurier, The wingmill: an oscillating-wing windmill, *Journal of Energy* 5 (1981) 109–115.
[3] K.H. Ly, V.A.L. Chasteau, Experiments on an oscillating-wing aerofoil and application to wing-energy converters, *Journal of Energy* 5 (1981) 116–121.
[4] J.F. Manwell, J.G. McGowan, A.L. Rogers, *Wind Energy Explained: Theory, Design and Application*, Wiley, New York, 2002.
[5] K.D. Jones, M.F. Platzer, Oscillating-wing power generator, in: *Proceedings of ASME/JSME-FEDSM99*, No. 7050, 1999.
[6] K.D. Jones, K. Lindsey, M.F. Platzer, An investigation of the fluid–structure interaction in an oscillating-wing micro-hydropower generator, in: S.K. Chakrabarti, C.A. Brebbia, D. Almorza, R.A. Gonzalez-Palma (Eds.), *Fluid Structure Interaction II*, WIT Press, Southampton, UK, 2003, pp. 73–82.
[7] K. Isogai, M. Yamazaki, M. Matsubara, T. Asaoka, Design study of elastically supported flapping wing power generator, in: *Proceedings of International Forum on Aeroelasticity and Structural Dynamics*, 2003.
[8] M. Matsumoto, Y. Honmachi, K. Okubo, Y. Ito, Fundamental study on the efficiency of power generation system by use of the flutter instability, *Proceedings of PVP2006-ICPVT-11*, No. 93773, 2006.
[9] A. Lee, Extraction of energy from flowing fluids, Canadian Patent No. 2266632, 2004.
[10] J.J. Allen, A.J. Smits, Energy harvesting eel, *Journal of Fluids and Structures* 15 (2001) 629–640.
[11] G.W. Taylor, J.R. Burns, S.A. Kammann, W.B. Powers, T.R. Welsh, The energy harvesting eel: a small subsurface ocean/river power generator, *IEEE Journal of Oceanic Engineering* 26 (2001) 539–547.
[12] C.B. Carroll, Energy harvesting eel, United States Patent No. 6424079, 2003.
[13] Humdinger Wind Energy, LLC., Technical Brief of Windbelt, 2008, see also URL ⟨http://www.humdingerwind.com⟩.
[14] Vortex Oscilation Technology, Ltd., Hydrogenerators with oscillating wings, 2008, see also URL ⟨http://www.vortexosc.com⟩.
[15] L. Tang, M.P. Païdoussis, On the instability and the post-critical behavior of two-dimensional cantilevered flexible plates in axial flow, *Journal of Sound and Vibration* 305 (2007) 97–115.
[16] T. Burton, D. Sharpe, N. Jenkins, E. Bossanyi, *Wind Energy: Handbook*, Wiley, New York, 2001.
[17] M.P. Païdoussis, *Fluid–Structure Interactions. Slender Structures and Axial Flow*, vol. 1, Academic Press, London, 1998.
[18] T. Balint, A.D. Lucey, Instability of a cantilevered flexible plate in viscous channel flow, *Journal of Fluids and Structures* 20 (2005) 893–912.
[19] J. Zhang, S. Childress, A. Libchaber, M. Shelley, Flexible filaments in a flowing soap film as a model for one-dimensional flags in a two-dimensional wind, *Nature* 408 (2000) 835–839.
[20] Y. Watanabe, S. Suzuki, M. Sugihara, Y. Sueoka, An experimental study of paper flutter, *Journal of Fluids and Structures* 16 (2002) 529–542.
[21] D.M. Tang, H. Yamamoto, E.H. Dowell, Flutter and limit cycle oscillations of two-dimensional panels in three-dimensional axial flow, *Journal of Fluids and Structures* 17 (2003) 225–242.
[22] M. Shelley, N. Vandenberghe, J. Zhang, Heavy flags undergo spontaneous oscillations in flowing water, *Physical Review Letters* 094302 (2005) 1–4.
[23] C. Eloy, R. Lagrange, C. Souilliez, L. Schouveiler, Aeroelastic instability of cantilevered flexible plates in uniform flow, *Journal of Fluid Mechanics* 611 (2008) 97–106.
[24] B.T. Benjamin, Dynamics of a system of articulated pipes conveying fluid. I. Theory, *Proceedings of the Royal Society (London) A* 261 (1961) 457–486.
[25] R.W. Gregory, M.P. Païdoussis, Unstable oscillation of tubular cantilevers conveying fluid. II. Experiments, *Proceedings of the Royal Society (London) A* 293 (1966) 528–542.
[26] M.P. Païdoussis, *Fluid–Structure Interactions. Slender Structures and Axial Flow*, vol. 2, Elsevier, Academic Press, London, 2004.
[27] M.J. Lighthill, Hydromechanics of aquatic animal propulsion, *Annual Review of Fluid Mechanics* 302 (1) (1969) 413–446.
[28] J.M. Anderson, K. Streitlien, D.S. Barrett, M.S. Triantafyllou, Oscillating foils of high propulsive efficiency, *Journal of Fluid Mechanics* 360 (1998) 41–72.
[29] M.S. Triantafyllou, G.S. Triantafyllou, D.K.P. Yue, Hydrodynamics of fishlike swimming, *Annual Review of Fluid Mechanics* 202 (2000) 3431–3438.
[30] L. Tang, M.P. Païdoussis, J. Jiang, The dynamics of variants of two-dimensional cantilevered flexible plates in axial flow, *Journal of Sound and Vibration* 323 (2009) 214–231.
[31] H.A. Sodano, D.J. Inman, G. Park, A review of power harvesting from vibration using piezoelectric materials, *The Shock and Vibration Digest* 36 (2004) 197–205.